Unsteady Shear of Dense Assemblies of Cohesive Granular Materials under Constant Volume Conditions

Lee R. Aarons, Jin Sun, and Sankaran Sundaresan*

Department of Chemical Engineering, Princeton University, Princeton, New Jersey 08544

The response characteristics of dense assemblies of cohesive granular materials to unsteady simple shear in the quasi-static regime are investigated through discrete element method (DEM) simulations of monodisperse spherical and frictional particles in periodic domains at constant volume. The dynamics of the volume-averaged normal and shear stresses in materials, undergoing stop-and-go shearing and oscillatory shear, are studied in detail. Furthermore, the evolution of microstructure anisotropy has been quantified through a fabric tensor. The stresses and the microstructure anisotropy depend on the strain extent but not on the shear rate. They both undergo a transition following reversal of shear direction, which requires a shear strain of order unity to fully adapt. The results reveal a correlation between the stress evolution and the microstructure anisotropy development.

1. Introduction

It is well-known that assemblies of granular materials behave differently under different flow conditions. Under rapid flow conditions, the particles interact with each other predominantly through binary collisions, while at slow shear rates the interaction is dominated by enduring contacts. In this paper, we focus on the rheological behavior of slowly deforming assemblies of granular materials.

Dense granular materials under steady shear have been studied extensively via simulations (e.g., see refs 1−5) and experiments (e.g., see refs 6−10). Campbell[11,12] carried out discrete element method (DEM) simulations of sheared assemblies of cohesionless particles in periodic domains and presented a map of the different regimes of flow. From these simulations, Campbell concluded that in the absence of gravity and interparticle cohesion, the quasi-static regime, where the stress has a negligible dependence on shear rate, only existed for very densely packed assemblies. Similar *steady shear* simulations performed for *cohesive* granular materials[13,14] revealed that interparticle attractive forces expand the range of volume fractions and shear rates over which the quasi-static flow regime is observed.

These studies only provide insight into shear at *constant* rates. However, granular materials are in general subjected to unsteady perturbations in nature and in industrial applications. It is thus of interest to investigate how granular systems respond under unsteady shear. Previous experimental work on unsteady shear has been done by Toiya et al.[15] using a Taylor−Couette-type shear cell. They measured shear forces and particle motion during a single and repeated shear reversals. They found that when shear was restarted in the same direction, the shear force rapidly attained its previous steady-state value; in contrast, if the shear direction was reversed, the material went through a transient period during which the shear force was small, the material compacted, and the shear band widened. The transient behavior was also observed in the velocity profile changes from cyclic shear experiments using a parallel plate device.[16]

It is worth noting that the transient stress response was first reported by Gadala-Maria and Acrivos[17] for unsteady shear of a suspension of noncolloidal particles. They measured the shear stress response to a single shear reversal and to sinusoidal shear using a parallel plate rheometer. After the direction of shear was reversed, the stress returned to its steady-state value only after a significant strain extent. This phenomenon was subsequently confirmed by other suspension experiments. Kolli et al.[18] and Narumi et al.[19] measured the normal stress as well as shear stress responses of suspensions to shear reversal in a parallel ring and in a parallel plate device, respectively. They found that the stress responses depended on the direction in which shear was restarted and that the data from different strain rates collapsed when plotted against strain. Narumi et al.[20] measured strain rate response of a suspension to large amplitude sinusoidal shear using a stress-controlled cone-and-plate rheometer. The characteristic strain scale for the stress to return to the steady value was about two for most of the suspensions.

Such transient response has been attributed to the rearrangement of the shear-induced anisotropic microstructure after shear reversal.[15,17] In fact, an anisotropic force network has been shown to form during steady shear of photoelastic disks in a two-dimensional (2D) biaxial cell[10] and a Couette geometry.[21] Strong force chains were found to form at approximately 45° to the flow direction under steady shear. They were weakened while the overall force network remained largely unchanged during the period when shear stopped. Shear reversal led to a transition, upon which the strong force chains switched to a direction normal to the previous strong force chain direction.[21]

From a constitutive modeling point of view, accurate measurements of the rheological responses and microstructure dynamics are also in great need. Such data can be used to develop constitutive models that can accurately predict the complex unsteady rheological behaviors by taking account of the microstructure dynamics. Previously, plasticity models have been used for quasi-static granular flows. For example, a Mohr−Coulomb yield criterion was used to derive a rigid plasticity model for flow down a rough inclined plane.[22] A von Mises-type yield function was used in derivation of another rigid perfectly-plastic model for analysis of instability of hopper flows.[23] These model were applicable only to incompressible flows. Critical state soil mechanics models were formulated to predict volume fraction changes associated with loading histories.[24] However, they are not applicable to cyclic loading

* To whom correspondence should be addressed. E-mail: sundar@princeton.edu.

10.1021/ie901187w
Published on Web 11/18/2009

conditions, and they do not adequately model stress-induced anisotropy. A constitutive model with microstructural anisotropy incorporated is promising in addressing these shortcomings.

While the above experimental data have provided some macroscopic rheological responses and microstructure dynamics of granular materials under unsteady shear, it is difficult to measure both under homogeneous deformation over large strain scales. For example, in all three granular shear experiments,[15,16,21] shear bands were formed with inhomogeneous velocity profiles across the gradient direction. This inhomogeneity predicates direct use of the data for constitutive model development, for which homogeneous deformation is often assumed in order to obtain the stress and strain information.[25] In addition, the microstructure is difficult to probe and quantify experimentally in three dimensions.

In this paper, the dynamics of normal and shear stresses in dense cohesive granular materials subjected to unsteady shear under constant volume conditions have been probed using DEM simulations. The constant volume conditions allow us to obtain the critical states and to study the microstructure evolution independently of dilation. Transient and sinusoidal oscillatory shear under (nearly) homogeneous deformation have been studied. A homogeneous velocity profile was always maintained to a very good approximation, except for slight perturbations at very small strain scales immediately after shear reversal and large step changes in shear rate magnitude; so the results could be used directly to aid constitutive model development.

It will be shown that the responses are indeed strain-rate-independent and strain-controlled, consistent with the experiments mentioned above. A robust characteristic strain scale of order unity was found to be necessary for the granular system to return to the steady state after shear reversal. It is also our goal to quantify the microstructure dynamics and correlate the microstructure evolution to the stress transition. The state of the microstructure has been quantified through the use of statistics of the orientation of the contacts, $\langle \hat{\mathbf{n}}_{p,c}\hat{\mathbf{n}}_{p,c}\rangle$, where $\hat{\mathbf{n}}_{p,c}$ is the unit normal vector pointing outward from particle p at contact c and the brackets signify a volume average. This quantity is associated with a symmetric second-rank fabric tensor, R, which indicates the anisotropy of the microstructure, as commonly used for granular materials.[26−28] We compute R directly from the contact information obtained from our simulations and use it to demonstrate that the microstructure evolves at the same order of strain scale as the stresses during unsteady shear. It thus provides a micromechanical basis and data for constitutive models using the fabric as an internal variable.[29−31] Implications of these results on constitutive modeling of quasi-static granular flows will also be discussed.

In section 2, the simulation methods and procedures for unsteady shearing are described. The results of theses simulations are discussed in section 3. The main results of this study are summarized and conclusions are drawn in section 4.

2. Details of Discrete Element Simulations

In this paper, the behaviors of cohesive materials undergoing different types of unsteady shear in the quasi-static regime are explored. Results of DEM simulations of steady shear under constant volume and constant applied normal stress conditions have already been described in our earlier publications.[13,14] The present study was devoted to DEM simulations of unsteady shear flow under conditions of constant volume. Two types of unsteady shear have been analyzed: shear with a square wave shear rate (i.e., "stop-and-go" shear), and oscillatory shear with a sinusoidal shear rate. The stress and fabric tensors were calculated throughout the shearing process for assemblies with different dynamic shear rates, levels of cohesion, and solid volume fraction (ϕ). These data were analyzed to determine how they evolved with time and how this evolution depended on system variables.

Simulations featured 2000 monodisperse, spherical particles with diameter d and density ρ. As generally done in DEM simulations, the particles were allowed to overlap when they collided, at which point the particles exerted a repulsive force on each other. The component of this force that would act in the normal direction (i.e., along the line connecting the particles' centers) is given by the linear (Hookean) spring−dashpot normal force model,

$$F_{\mathrm{n}} = k\alpha - \eta v_{\mathrm{n}} \tag{1}$$

where k is the normal spring stiffness, α is the overlap, η is the damping coefficient, and v_{n} is the relative normal velocity of the colliding particles.[32] The damping term is the source of inelasticity in this model; the elasticity can be quantified using the coefficient of restitution, defined as the ratio of the relative rebound speed to the relative impact speed, given for the linear spring−dashpot model by

$$\varepsilon = \exp\left(-\frac{\pi\eta}{\sqrt{2mk - \eta^2}}\right) \tag{2}$$

where $m = \pi\rho d^3/6$ is the mass of a particle.[33,34]

The force exerted by colliding particles in the tangential direction, as the surfaces rub against each other, is given by a linear spring−slider model,[35,36]

$$F_{\mathrm{t}} = \min(k_{\mathrm{t}}\Delta s, \mu F_{\mathrm{n}}) \tag{3}$$

Here k_{t} is the tangential spring constant and Δs is the distance the surface of one particle moves relative to the other in the tangential direction. The force is limited by a Coulombic upper bound, given by μF_{n}, where μ is the interparticle friction coefficient.

When cohesive particles were simulated, they also interacted with each other via the van der Waals force. A pair of particles with a Hamaker constant A and surfaces separated by a distance s would attract each other with a van der Waals force with a magnitude of[37]

$$F_{\mathrm{vdW}} = \frac{Ad^6}{6s^2(s+2d)^2(s+d)^3} \tag{4}$$

which reduces to the more familiar expression, $F_{\mathrm{vdW}} = Ad/24s^2$, when $s \ll d$. This model diverges when particles collide, and to avoid this, a minimum cutoff separation, $s_{\min}$, was used, such that when $s < s_{\min}$, the van der Waals force remained equal to the force experienced at $s_{\min}$. Previous simulations have used values of 0.4[38] and 1 nm[37] for $s_{\min}$, corresponding to typical intermolecular distances. In the simulations described in this paper, a minimum cutoff of $4 \times 10^{-5}d$ had been used, and so, the simulated particles can be assumed to have diameters between 10 and 25 μm. Since the van der Waals force drops off rapidly with increasing separation, in order to speed up the simulation, there was a maximum cutoff separation equal to $d/4$, beyond which the cohesive force was ignored. The strength of cohesion is commonly expressed in dimensionless form as the Bond number, Bo, is commonly used as defined as the ratio of the maximum van der Waals force experienced by a particle (i.e., at contact) to its weight. However, the simulations were performed in the absence of gravity, and so, a modified Bond number, which compares the van der Waals force to a

Table 1. DEM Computational Parameters[a]

interparticle normal stiffness coefficient	k_n	100000
interparticle tangential stiffness coefficient	k_t	$2/7k_n$
interparticle friction coefficient	μ	0.1
interparticle restitution coefficient	ε	0.7
Hamaker constant	A	1.92×10^{-9}, 9.6×10^{-8}, 4.8×10^{-7}
particle diameter	D	1
particle density	ρ	1
minimum separation between particles	s_{min}	4×10^{-5}
applied shear rate	$\dot{\gamma}$	$10^{-1.5}-10^{-2.5}$

[a] The dimensional parameters involved in dimensionless groups, k^* and Bo^*, are presented in forms without any units because their physical significance can only be assessed by the magnitudes of those dimensionless groups in our simulations.

characteristic contact force, was used instead: $Bo^* = F_{vdw}^{max}/kd \approx A/24ks_{min}^2$. The systems presented in this paper were simulated with at least one of three levels of cohesion: $Bo^* = 5 \times 10^{-7}$, 2.5×10^{-5}, and 1.25×10^{-4}. For simplicity, these levels of cohesion will be referred to in figures as LC (low cohesion), MC (medium cohesion), and HC (high cohesion), respectively. In this paper, we only show results for assemblies at lower volume fractions that are in the quasi-static regime only when cohesive particles are used. Cohesive assemblies at higher volume fractions exhibit similar characteristics regarding the quasi-static rheological behaviors discussed here. For cohesionless granular assemblies in quasi-static flow, the stress and microstructure evolutions have qualitatively the same trends; the primary effect of cohesion is simply to allow quasi-static flow to occur at lower volume fractions.[13,14] Thus the results for cohesionless particles will not be presented in this paper. The computational parameters used in the DEM simulations are listed in Table 1.

The particles existed in three-dimensional (3D) periodic cubic boxes of length H. Shear was induced via the Lees−Edwards boundary conditions,[39] with the stream velocity in the x-direction and the velocity gradient in the z-direction. The use of these boundary conditions by themselves would imply that, when the shear rate changes during the course of a simulation, only the particles at the top and bottom of the domain would immediately "feel the effect" of the shear rate change. It would take some nonzero time for the rest of the particles to "be aware" of the change. Thus after a change in shear rate, the shear would not be homogeneous, such that different layers of particles would be experiencing different shear rates.

This effect can be greatly reduced through the use of the SLLOD algorithm.[40] The SLLOD algorithm implies that a change in shear rate is not achieved by simply moving the boundaries of the system faster or slower, but by applying a force to the entire system. At a distance z from the bottom of a homogeneously sheared system, the mean velocity is given by

$$\mathbf{u} = \left(z - \frac{H}{2}\right)\dot{\gamma}\hat{x} \tag{5}$$

(such that at $z = H/2$, the mean streaming velocity is zero). Thus the force applied to every particle every time the shear rate changes would be given by

$$\mathbf{F}_{SLLOD} = m\left(z_p - \frac{H}{2}\right)\frac{d\dot{\gamma}}{dt}\hat{x} \tag{6}$$

where m is the mass of a particle and z_p is the z-coordinate of the particle's position measured from the bottom of the domain. It can be seen that if a particle is traveling at a velocity corresponding to homogeneous shear and is not interacting with any other particles (i.e., it is experiencing no forces), the application of the SLLOD algorithm when the shear rate is changed will cause the particle to immediately move at a velocity corresponding to the new shear rate. By using the SLLOD algorithm, a system at any point in time (ideally) can be described by a single stress tensor and shear rate, rather than a layer-by-layer description. Thus, the results from using the SLLOD algorithm are useful for the construction of constitutive models, and all the results presented here are from simulations that used SLLOD.

Periodically throughout the simulations, the stresses arising from interparticle forces and velocity fluctuations were calculated and recorded. For a volume V consisting of N particles, this stress due to interparticle forces is defined as[1]

$$\sigma^{ip} = \frac{1}{V}\sum_{p=1}^{N}\sum_{q\neq p}^{N} l_{pq}f_{pq} \tag{7}$$

The branch vector l_{pq} connects the center of particle p to the midpoint of particles p and q. The force vector f_{pq} is the total force particle p exerts on particle q, which is the sum of van der Waals force and the spring−dashpot force.

The stress arising from velocity fluctuations, i.e. the energy that is not directly generated by shearing, referred to as the momentum flux, is defined as

$$\sigma^{mf} = \frac{1}{V}\sum_{p=1}^{N}\frac{\pi}{6}\rho d^3\left(v_p - \dot{\gamma}\left(z_p - \frac{H}{2}\right)\hat{x}\right)\left(v_p - \dot{\gamma}\left(z_p - \frac{H}{2}\right)\hat{x}\right) \tag{8}$$

Here, v_p is the velocity of particle p, z_p is the z-component of the position vector of particle p, and $\hat{x}$ is the unit vector in the x-direction. In homogeneous shear, the average velocity of a particle located at height z_p would be $\dot{\gamma}(z_p - (H/2))\hat{x}$. The total stress, σ, would then be the sum of the stress due to interparticle forces and the momentum flux. The dimensionless, or scaled, stress is given by $\sigma d/k$. Though the stress tensor has, of course, three normal components, for simplicity the term "normal stress" will refer to the zz-component unless otherwise noted. Similarly, "shear stress" will refer to the xz-component of the stress tensor.

The first type of unsteady simulations that will be described below is "stop-and-go shearing". In these simulations, systems were first sheared at some initial (constant) shear rate, $\dot{\gamma} = \dot{\gamma}_0$, for several box lengths. Then, the shear rate was reduced to zero instantaneously (at $t = -1/\dot{\gamma}_0$) and kept at zero for a time, $t = 1/\dot{\gamma}_0$ (i.e., equivalent to the time it would take to reach a strain of unity at a shear rate $\dot{\gamma}_0$). Next, shearing was resumed (at $t = 0$) at the original shear rate in the original direction ($\dot{\gamma} = \dot{\gamma}_{new} = \dot{\gamma}_0$) or in the opposite direction ($\dot{\gamma} = \dot{\gamma}_{new} = -\dot{\gamma}_0$), for several box lengths. Figure 1a shows how the shear rate varies with time for these simulations. For these systems, we define a "directional scaled stiffness", $K = (\dot{\gamma}_{new}/\dot{\gamma}_0)k^*$, that is identical to a dimensionless "scaled stiffness", $k^* = k/\rho d^3\dot{\gamma}^2$, except that its sign indicates the direction of shear when it is resumed. Thus when K is positive, shear is resumed in the original direction, and when it is negative, the shear direction is reversed.

Oscillatory shear simulations will then be described. In these simulations, the shear rate varied sinusoidally with time, t:

$$\dot{\gamma}(t) = \dot{\gamma}_{max}\sin(\omega t) \tag{9}$$

Here $\dot{\gamma}_{max}$ is the maximum shear rate and ω is the frequency of the oscillations, such that the period of oscillation is $2\pi/\omega$. These two parameters were varied to determine their effect on the

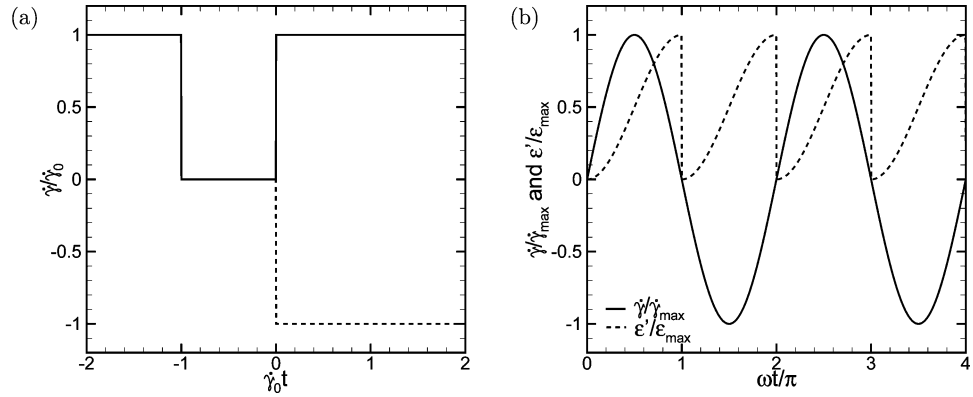

Figure 1. Time dependence of the shear rate for the two different types of unsteady shear: (a) stop-and-go shear and (b) oscillatory shear. In part a, the shear rate reduced by the original shear rate ($\dot{\gamma}/\dot{\gamma}_0$) is plotted against the dimensionless time, $\dot{\gamma}_0 t$; the solid lines represent the shear rate before the step change, and the dashed and dotted lines represent the shear rate after the step change. In part b, the shear rate reduced by the maximum shear rate ($\dot{\gamma}/\dot{\gamma}_0$, solid line) as well as the strain reduced by the maximum strain ($\varepsilon'/\varepsilon'_{max}$, dashed line) are plotted against the number of half-periods of oscillation completed ($\omega t/\pi$).

systems' behavior. We can define three different strains for these simulations. The first is relative to the state at $t = 0$:

$$\varepsilon(t) = \int_0^t \dot{\gamma}(t')\,dt' = \frac{\dot{\gamma}_{max}}{\omega}(1 - \cos(\omega t)) \tag{10}$$

This gives a maximum strain of

$$\varepsilon_{max} = \frac{2\dot{\gamma}_{max}}{\omega} \tag{11}$$

Given that the shear starts out at $t = 0$ in the positive x-direction, this strain goes from 0 to ε_{max} as shear proceeds in the positive direction, and then it goes from ε_{max} to 0 as shear proceeds in the negative direction. However, as it will be shown later, the stress evolution is not symmetric about the flow-reversal point, and a modified strain, ε', that goes from 0 to ε_{max} regardless of the direction of shear, defined below, is more useful for capturing the simulation results.

We can also define an accumulated strain, ε_{total}, such that, when shear is reversed, it is not reset to zero and shearing in any direction increases the strain. This is equivalent to using the absolute value of the shear rate to define strain:

$$\varepsilon_{total}(t) = \int_0^t |\dot{\gamma}(t')|\,dt' = \frac{\varepsilon_{max}}{2}\left(1 - \cos\left(\omega t - \pi\left\lfloor\frac{\omega t}{\pi}\right\rfloor\right) + 2\left\lfloor\frac{\omega t}{\pi}\right\rfloor\right) = \varepsilon' + \varepsilon_{max}\left\lfloor\frac{\omega t}{\pi}\right\rfloor \tag{12}$$

As π/ω is equal to half of the period of oscillation, $\lfloor(\omega t/\pi)\rfloor$ is the integer number of half-oscillations that have been completed by time t. From eq 5, we get

$$\varepsilon' = \frac{\varepsilon_{max}}{2}\left(1 - \cos\left(\omega t - \pi\left\lfloor\frac{\omega t}{\pi}\right\rfloor\right)\right) \tag{13}$$

For the rest of this paper, the term strain will refer to the quantity defined by eq 13 rather than eq 10, and total strain will refer to the quantity defined in eq 12. Figure 1b shows how $\dot{\gamma}$ and ε' vary with time for these simulations.

For oscillatory shear, a system can be identified by a "reduced minimum scaled stiffness", $\kappa = 10^{-8}k/\rho d^3\dot{\gamma}_{max}{}^2$, and maximum strain, ε_{max}. (The factor 10^{-8} is used in the definition of κ so that, for the oscillatory shear systems discussed here, κ is between 3 and 100.)

The results presented in this paper take the form of stress (specifically the normal and shear stresses), fabric tensor (generally the shear component), and average coordination number (i.e., the average number of contacts per particle, Z) versus some measure of strain. As mentioned above, we use the total strain, ε_{total}, for oscillatory shear, such that we examine how the system behavior evolves with the total distance sheared since the start of shear. For those simulations that feature stop-and-go shearing, we are most interested in describing the system behavior after shear is resumed, and so in these cases, it is most convenient to define the strain as $\gamma_0 t$, where $t = 0$ is identified as when shear is resumed after stopping. This quantity is thus equivalent to the strain experienced after shear resumes when $t \geq 0$ but is just a dimensionless time when $t < 0$. Similarly, for those simulations in which a single step change in shear rate occurs, we are most interested in the behavior after the step change occurs, and so, we define the strain as $\dot{\gamma}_{new} t$, where $t = 0$ is identified as when the step change occurs. Again, this quantity is equivalent to the strain experienced after the step change occurs when $t \geq 0$ but is just a dimensionless time when $t < 0$.

The fabric tensor is computed as

$$R = \frac{\phi}{N}\sum_{p=1}^{N}\sum_{c>p}^{N}\hat{\mathbf{n}}_{p,c}\hat{\mathbf{n}}_{p,c} \tag{14}$$

for monodisperse collections of particles. Here ϕ is the solid volume fraction, N is the number of particles. It can readily be shown that the trace of the fabric tensor is equal to the product of the volume fraction and average coordination number (ϕZ). Furthermore, the eigenvectors of the fabric tensor give the principal directions of the mean contact orientations. The eigenvalues, in turn, provide a measure of the extent of contact orientations along the principal directions. If the three eigenvalues are all equal, then the orientation is not pointed in one principal direction more than another, and so, we say the contact orientation is isotropic. As the eigenvalues become more different, the contacts tend to become more oriented in the direction of the eigenvector corresponding to the largest eigenvalue, and so, the structural anisotropy increases.

That being said, the structural anisotropy can easily be related to the shear (xz-)component of the fabric tensor for simple shear flows. To demonstrate this, we show the different components of the fabric tensor for one case of stop-and-go shearing in which the direction of shear is reversed when resumed in Figure 2a and b. By scaling the normal components shown in Figure 2a by ϕZ, it can be seen that at all times the three normal components are approximately equal to one-third of ϕZ. Furthermore, of all the off-diagonals shown in Figure 2b, only the xz-component is nontrivial. These observations hold true during steady state before shear becomes unsteady, immediately

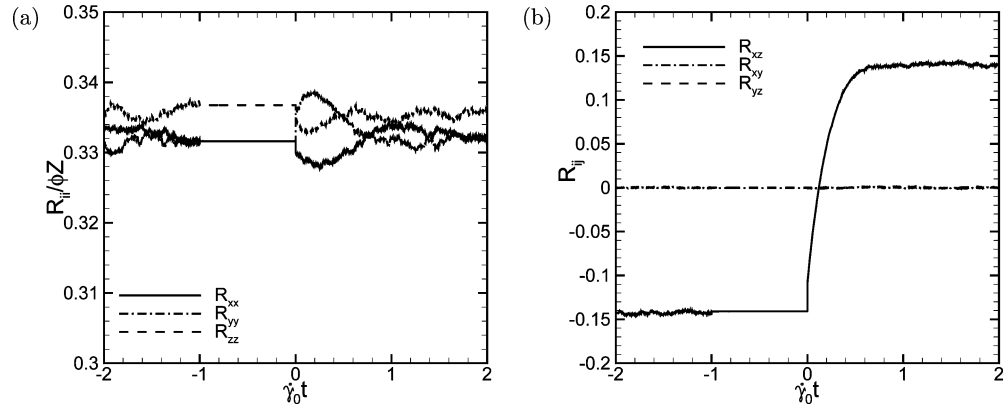

Figure 2. Evolution of the fabric tensor of a system subjected to stop-and-go shearing. Plotted are (a) the normal components of the fabric tensor (R_{xx}, R_{yy}, and R_{zz}) scaled by the product of the volume fraction and average coordination number (ϕZ) and (b) the off-diagonal components of the fabric tensor (R_{xy}, R_{xz}, and R_{yz}) versus the dimensionless time, $\dot{\gamma}_0 t$, for a system with $K = -10^9$, $\phi = 0.6$, and $Bo^* = 2.5 \times 10^{-5}$.

following changes in shear rate, and long afterward. So to a good approximation, in all our simulations,

$$R \approx \begin{pmatrix} \phi Z/3 & 0 & R_{xz} \\ 0 & \phi Z/3 & 0 \\ R_{xz} & 0 & \phi Z/3 \end{pmatrix} \tag{15}$$

which has major and minor eigenvalues separated by $2R_{xz}$. Thus, the structural anisotropy increases with the magnitude of R_{xz}. Also, the sign of R_{xz} provides the preferred contact orientation. The preferred orientation is always in the xz-plane, at an angle of $\pm 45°$ to the x-axis; the largest eigenvalue, and hence the preferred orientation, corresponds to a positive (negative) angle when R_{xz} is positive (negative).

In our previous studies,[13,14] all the results were obtained from simulations generated by internally developed code. However, the results discussed here were obtained from simulations generated by an open source code, LAMMPS (large-scale atomic/molecular massively parallel simulator), created at Sandia National Laboratories, as LAMMPS proved to be significantly faster.[41] We reproduced the steady-shear results discussed in our previous publications[13,14] with LAMMPS. Furthermore, some of the results discussed in this paper were also reproduced using our internally developed code, as further verifications of the simulations. All the results presented in this paper were simulated with multiple initial configurations to generate 20 realizations for the stop-and-go shearing and 10 realizations for

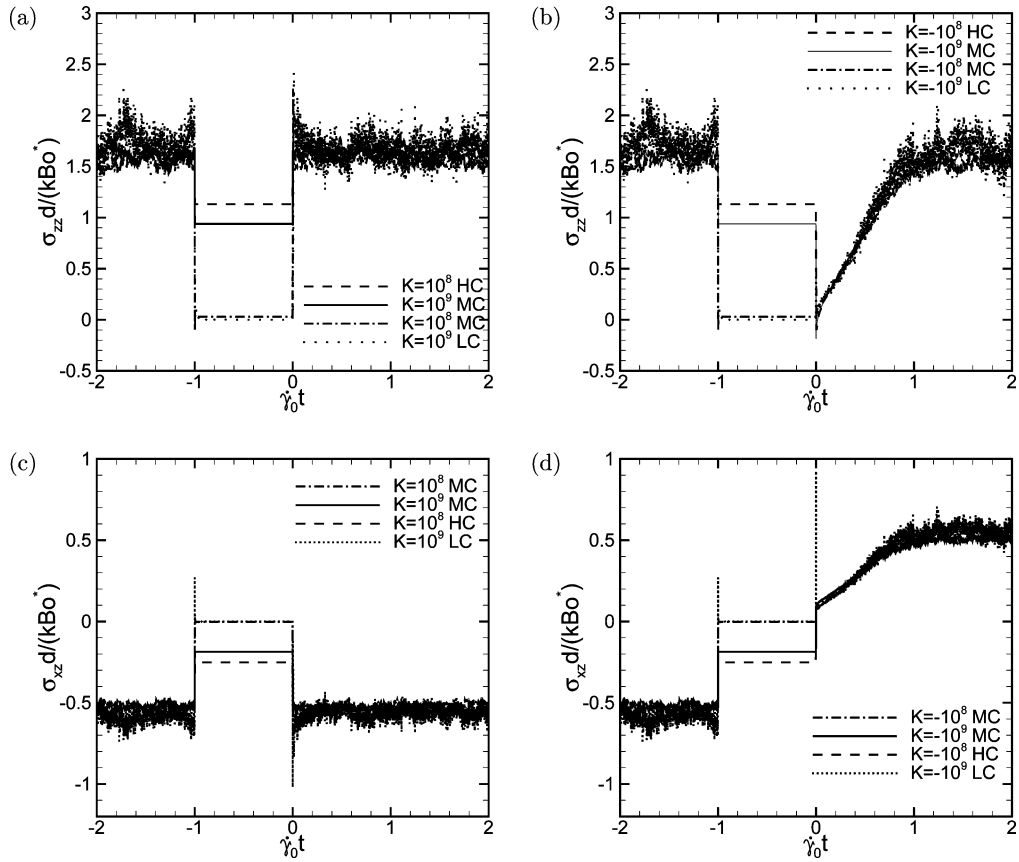

Figure 3. Evolution of the stress of systems subjected to stop-and-go shearing. Plotted are the cohesively scaled normal stress ($\sigma_{zz}d/(kBo^*)$) and shear stress ($\sigma_{xz}d/(kBo^*)$) versus the dimensionless time, $\dot{\gamma}_0 t$, for systems in which the shear is stopped and then resumed at the original shear rate in the original direction (a and c) and in the opposite direction (b and d). In all cases, shear is stopped at $\dot{\gamma}_0 t = -1$ and resumed at $\dot{\gamma}_0 t = 0$; $\phi = 0.6$.

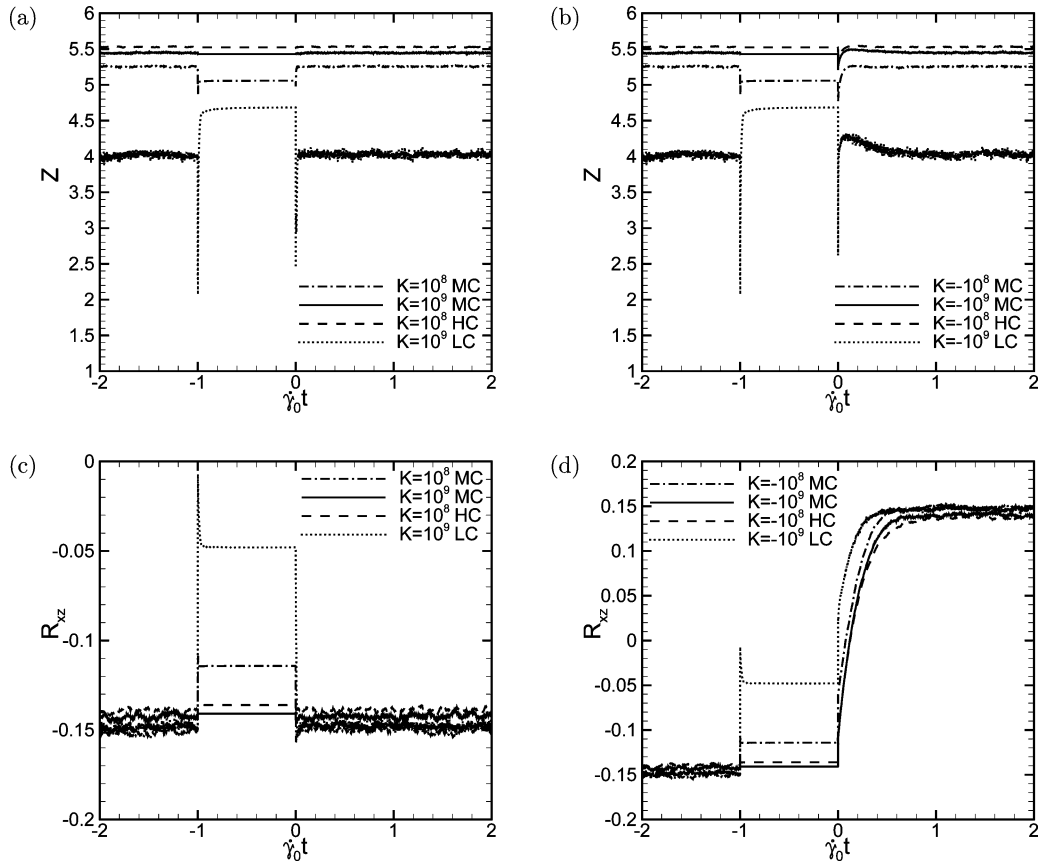

Figure 4. Evolution of microstructure of systems subjected to stop-and-go shearing. Plotted are the average coordination number (Z) and the shear component of the fabric tensor (R_{xz}) versus the dimensionless time, $\dot{\gamma}_0 t$, for systems in which the shear is stopped and then resumed at the original shear rate in the original direction (a and c) and in the opposite direction (b and d). In all cases, shear is stopped at $\dot{\gamma}_0 t = -1$ and resumed at $\dot{\gamma}_0 t = 0$; $\phi = 0.6$.

the oscillatory shearing; the results were then averaged over these realizations.

3. Results and Discussion

3.1. Stop-and-Go Shearing. Figures 3 and 4 show how the normal stress, shear stress, average coordination number, and shear component of the fabric tensor (R_{xz}) evolve with strain for cohesive assemblies in the quasi-static regime with $\phi = 0.6$ subjected to stop-and-go shearing. The volume fraction was chosen so that the quasi-static regime was reached. The specific value was obtained from previous simulations on quasi-static flows reported in our previous work.[13] As long as the flow is in the quasi-static regime, the change of volume fraction will not change the trends observed here but only the stress magnitudes. In each figure, panels a and c show the behavior for the cases where shear is stopped and then resumed in the original direction, while panels b and d show the behavior for the cases where shear is stopped and then resumed in the opposite direction. As observed in a previous study,[13,14] the steady state stress scales with Bo^* in this regime. Thus, the stresses in Figure 3 are scaled by Bo^* to compare results for systems with different levels of cohesion as well as different shear rates (or equivalently, different k^*). The dynamic responses of normal stresses, as well as the shear stresses, collapse into a single curve over all cases when scaled in this manner and plotted against strain. (Most of the stress fluctuations observed in Figure 3 were generated from the system with $K = \pm 10^9$ and LC, which will be explained later.) This confirms that the dynamics is controlled by the deformation strain and is strain-rate-independent. As mentioned before, anisotropic microstructure is formed at steady state, and as evidenced in Figure 4, R_{xz} has a steady-state magnitude of about 0.14 (though the actual steady-state R_{xz} varies slightly from system to system).

A salient feature of the response is that it depended on whether shear was resumed in the original direction or in the opposite direction. When shear was stopped at $\dot{\gamma}_0 t = -1$, the particles were more or less frozen in place; however, the slight rearrangement that occurred was enough to cause measurably large changes in the stresses, average coordination number, and R_{xz} (see Figures 3 and 4). When shear was resumed in the original direction (at $\dot{\gamma}_0 t = 0$), the stresses (Figure 3a and c) and microstructure (Figure 4a and c) returned to steady state almost instantaneously as the particles only needed to be moved a little to return to the steady-state microstructure.

On the other hand, when shear was resumed in the opposite direction, the particles needed to completely rearrange themselves to form force chains in the opposite direction, requiring shear to proceed much longer to reach steady state. As shear progressed, the normal and shear stresses increased nearly linearly with strain until steady state was achieved at around a strain of unity (Figures 3b and d); the evolution of the scaled stresses with strain extent was essentially independent of strain rate and cohesion. At the same time, the orientation of the contacts slowly reversed, as evidenced by R_{xz} gradually going from a negative value to a positive value (see Figure 4d), which indicates the microstructure rearrangement. The evolution of the structure with strain was virtually independent of shear rate and cohesion. However, as the value of R_{xz} in the "stop" phase of the simulation ($-1 < \dot{\gamma}_0 t < 0$) was different for each system before shear was reversed, the actual amount of strain required to reach the final steady state R_{xz} differed between the systems. Nevertheless, in all cases R_{xz} leveled out at strains between about

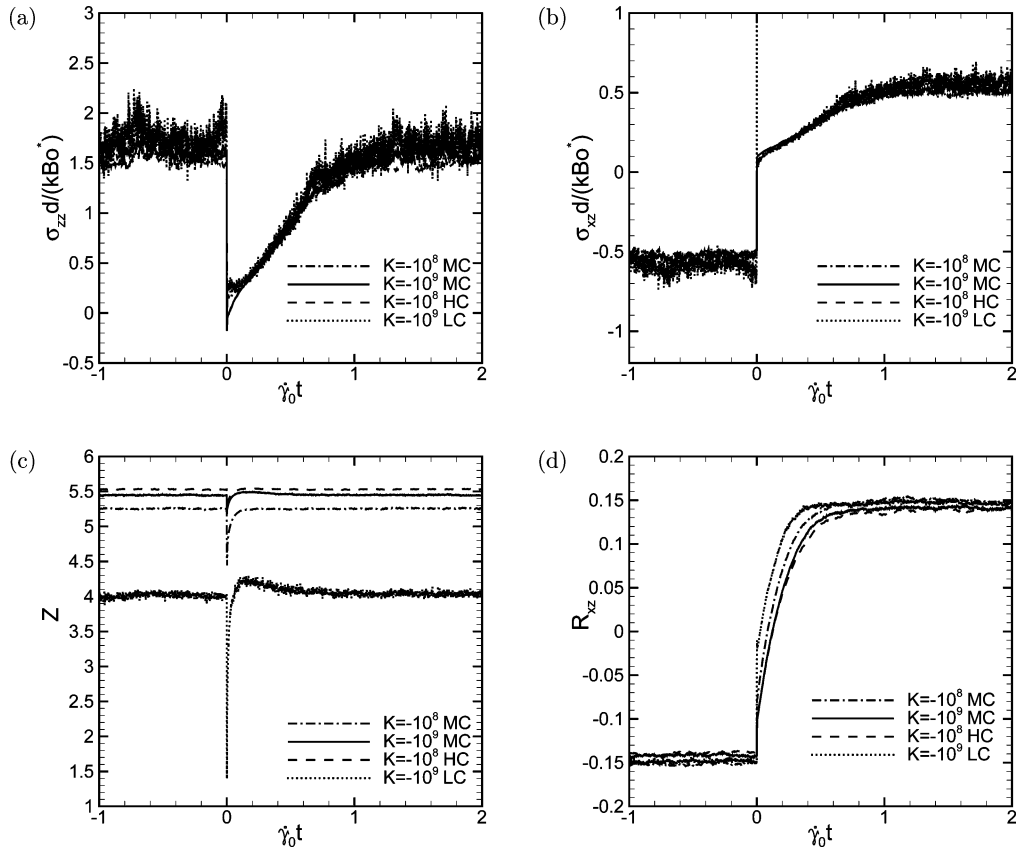

Figure 5. Evolution of the systems subjected to shear reversal without a stop phase. Plotted are (a) the cohesively scaled normal stress ($\sigma_{zz}d/(kBo^*)$); (b) the cohesively scaled shear stress ($\sigma_{xz}d/(kBo^*)$); (c) the average coordination number (Z); and (d) the shear component of the fabric tensor (R_{xz}) versus the dimensionless time, $\dot{\gamma}_0 t$. In all cases, shear is reversed at $\dot{\gamma}_0 t = 0$; $\phi = 0.6$.

0.5 and 0.7, i.e. before the stresses did. This implies that the microstructure needs to be in place for the force chains and stress to build up, and that it must be in place for a sufficient amount of strain for the stress to reach steady state. The anisotropy of microstructure also has been shown to evolve faster than the shear stress in dense suspensions as revealed by the pair distribution function evolution in Stokesian dynamics simulations of shear reversal.[42]

To determine how the differences between the curves seen in Figure 4d upon shear reversal are affected by the fact that the values of R_{xz} in the stop phase were different, simulations were repeated without a stop phase, where the assemblies were sheared in one direction until a statistical steady state was reached and then the shear was instantaneously reversed at $\dot{\gamma}_0 t = 0$. Figure 5a−d shows the normal and shear stresses, average coordination number, and the shear component of the fabric for such simulations and can be compared with panels b and d of Figures 3 and 4. As can be seen readily, the evolution of R_{xz} for the different simulations are now slightly closer to one another, confirming that the stop phase in Figures 3 and 4 was responsible for some of the differences seen among the different curves in Figure 4d.

The physical significance of unit strain required for the stress and microstructure evolution following shear reversal is easy to visualize. If we imagine the assembly of particles as layers of particles (with each layer in contact with the adjacent ones), unit strain corresponds to the translation of the particles in one layer by a distance of one particle diameter relative to the particles in the adjacent layer. In a more randomly configured assembly of particles, such a translation will involve particle *climbing over* a particle in an adjacent layer and this will naturally lead to normal stress variations.

The evolution of shear stress following stop-and-go shear presented here are remarkably similar to the experimental results reported by Gadala-Maria and Acrivos[17] for dense suspensions. The presence of the interstitial fluid in their experiments introduces lubrication stresses, which are not present in our simulations; yet, the similarity is so strong that the mechanisms discussed here are likely relevant for their system as well.

Figures 3 and 4 also show appreciable changes at small strain scales immediately following sudden changes; the mechanisms behind those responses can be explained as follows. It is first noted that these spikes and dips are not numerical artifacts resulting from incomplete resolution of the motions; simulations performed using several widely different time steps reproduced these features. The small strain scale responses depend on the level of cohesion and steady-state average coordination number, which in turn had an additional dependence on the level of cohesion as well as the scaled stiffness (see Figure 6 in ref 13). The coordination number characterizes the connectivity of a granular assembly.[43] When the coordination number is equal to the critical value Z_c (equal to 4 for 3D frictional particle assemblies studied here), the granular assembly is at an isostatic state, where the number of degrees of freedom is matched by number of constraints between particles. For coordination number $Z < Z_c$, the assembly cannot be stable and it will rearrange. For $Z > Z_c$, the assembly is overconnected and apt to resist external perturbations, thus stable. When shear came to an immediate halt, the assembly tended to relax as the external constraint to deformation was removed. The extent of the relaxation, however, depended on the stability of the assembly microstructure as indicated by the average coordination number.

Resuming shear in the original direction brought the stress instantly back to its steady state value for those cases in which

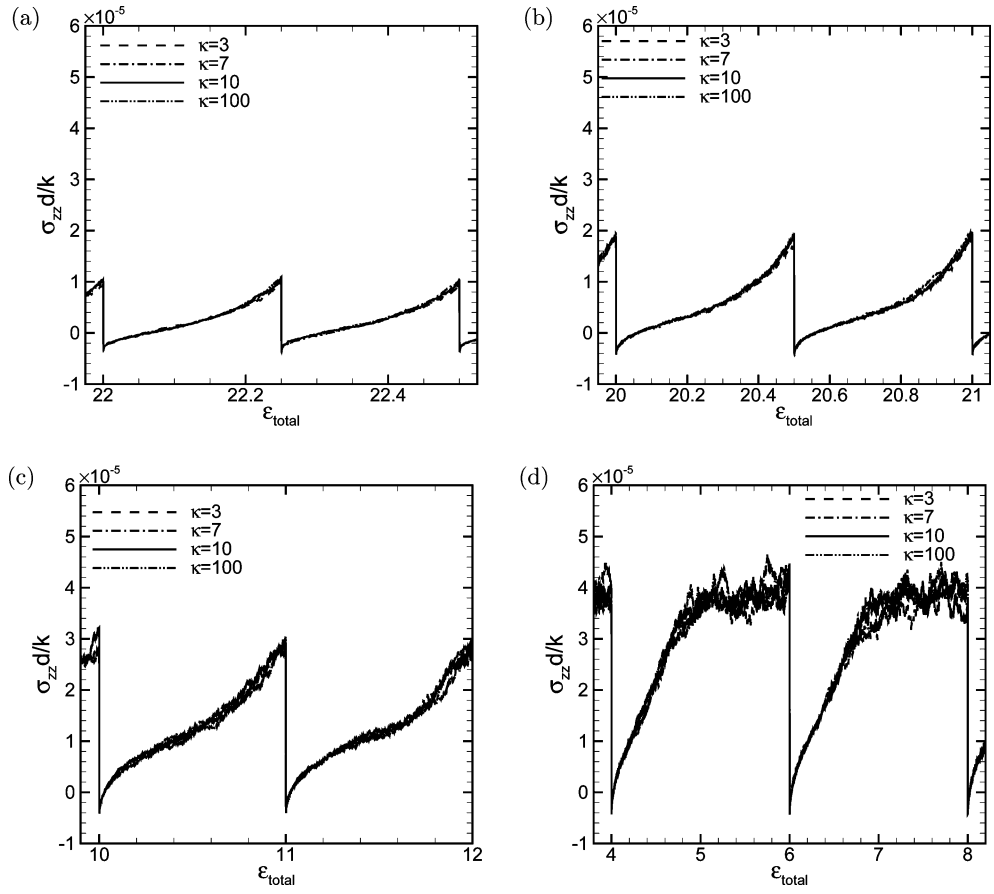

Figure 6. Strain dependence of the normal stress for oscillatory shear with maximum strains of (a) ε_{max}= 0.25, (b) ε_{max}= 0.5, (c) ε_{max}= 1, and (d) ε_{max}= 2. Plotted is the scaled normal stress ($\sigma_{zz}d/k$) versus the total strain (ε_{total}). Each figure features the stress evolution for four different values of the reduced minimum scaled stiffness (κ = 3, 7, 10, and 100). In all cases, ϕ = 0.6 and $Bo^* = 2.5 \times 10^{-5}$.

the average coordination numbers are high ($K = 10^8$ with HC and $K = 10^9$ with MC in Figure 3a and c), as the microstructure remained largely unchanged and no rearrangement was needed. In the other cases, the particles needed be rearranged slightly in order to return to steady state; first, the contacts formed after shear was stopped were destroyed, and then, the shear and cohesion reestablished the contacts in the original arrangement (as measured by R_{xz}, Figure 4c). As the particles hardly moved since shearing was stopped, this process was extremely quick. The process of breaking and reestablishing contacts so quickly led to a very short-lived spike in both the normal and shear stresses before steady state was achieved.

The moment shear was reversed, the shear stress became positive, but again, the specific behavior can be linked to the system history. For those systems exhibiting stable microstructures (high average coordination numbers; $K = -10^8$ with HC and $K = -10^9$ with MC), the reversal of shear essentially caused the force chains to be ripped apart as the anisotropy is destroyed, causing the stress to instantly drop and leading to a very short-lived tensile state (as seen as a negative normal stress in Figure 3b). This was of course an effect of using cohesive particles, as cohesion was the only source of a negative normal stress (aside from a negligible effect from the dashpot[13]). When shearing reversed direction, since the mean orientation of contacts gradually changed, the microstructure did not immediately conform to the new compression direction and most contacts remained in the previous direction, which was subjected to less compression after the shear direction reversed. (See, for example, the R_{xz} remained positive immediately after shear reversal in Figure 4d.) This microstructure transition led to the tensile state. However, in the other cases, the structures were not as difficult to rearrange and reversing shear did not lead to a tensile state. When cohesion was weak (LC, for which $Bo^* = 5 \times 10^{-7}$), the extra contacts formed needed to be destroyed, requiring a small spike in both the normal and shear stress. The spikes seen in Figure 5 are also explained in the same manner.

When shear was stopped, the stresses dropped significantly if the average coordination number prior to stopping was small ($K = \pm 10^8$ with MC and $K = \pm 10^9$ with LC in Figure 3). When the level of cohesion was large enough (MC, for which $Bo^* = 2.5 \times 10^{-5}$), this led to negative normal stress (at $\dot{\gamma}_0 t = -1$ in Figure 3a and b), i.e. the system was in tension as force chains were disrupted and the particles pulled each other back. The spikes can be explained similarly to the shear resuming cases discussed above. Furthermore, the magnitude of R_{xz} dropped when shear was stopped, as the breaking of force chains resulted in a loss of anisotropy (see Figures 4c and d).

3.2. Oscillatory Shear Results. Figures 6a−d show how the normal stress evolves with the total strain during the oscillatory shear of cohesive assemblies (with $Bo^* = 2.5 \times 10^{-5}$) at a volume fraction of 0.6 for four different values ε_{max}. Each figure features the stress evolutions for four different reduced minimum scaled stiffnesses, κ (defined earlier in section 2). (In all these figures, oscillatory shear was maintained for many cycles to ensure that little memory of the initial conditions for the simulations remained and a periodic solution which is representative of the long-time solution resulted.) As the shear rate increased from zero (i.e., starting from any point where ε_{total} is an integer multiple of ε_{max}), the normal stress rose. The steady-state normal stress could be achieved despite the constantly changing shear rate, provided the strain amplitude was suf-

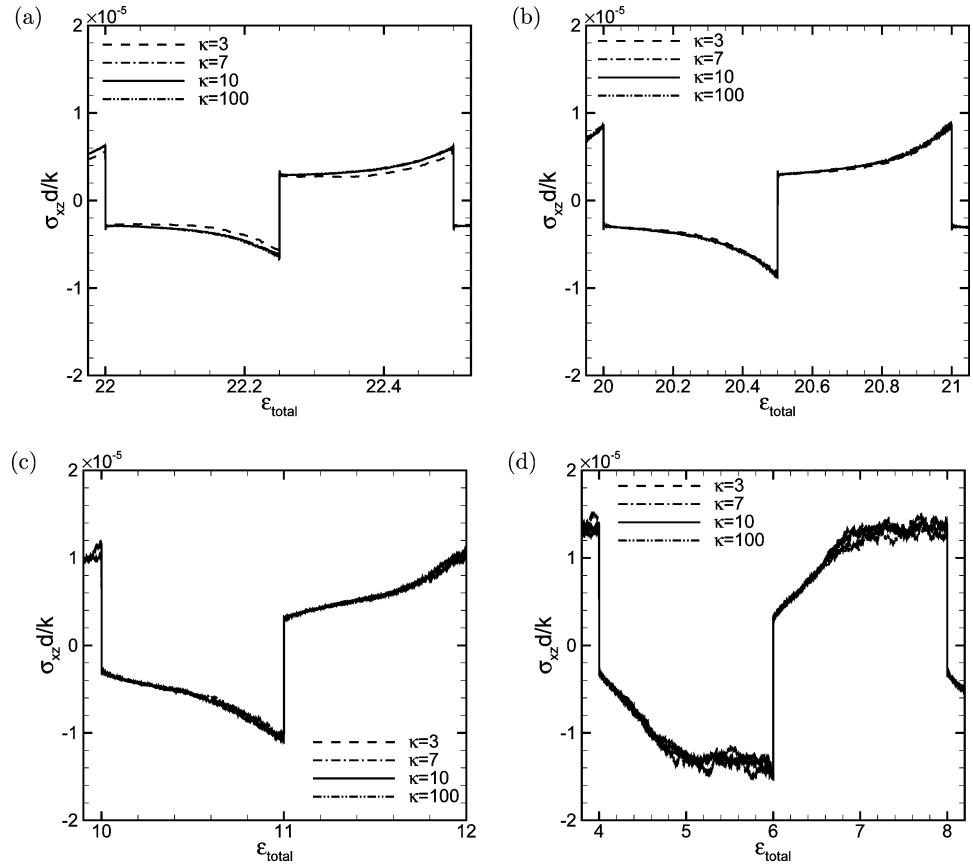

Figure 7. Strain dependence on the shear stress for oscillatory shear with maximum strains of (a) ε_{max}= 0.25, (b) ε_{max}= 0.5, (c) ε_{max}= 1, and (d) ε_{max}= 2. Plotted is the scaled shear stress ($\sigma_{xz}d/k$) versus the total strain (ε_{total}). Each figure features the stress evolution for four different values of the reduced minimum scaled stiffness (κ = 3, 7, 10, and 100). In all cases, ϕ = 0.6 and Bo^* = 2.5 × 10^{-5}.

ficiently larger than unity (see Figure 6d corresponding to strain amplitude of 2). When the strain amplitude was smaller (Figure 6a−c), steady state (i.e., plateau region in the stress) was clearly not reached.

Figure 7a−d shows the shear stress evolution for those systems in Figures 6a−d, respectively. The sign of the shear stress depends on the direction of shear, just as in steady shear, whereas obviously the normal stress does not. It is clear from Figure 7 that when the direction of shear was changed, the shear stress changed sign almost immediately and assumed a significant magnitude; subsequently, the magnitude of the shear stress continued to evolve slowly, reaching a plateau when the strain amplitude was in excess of unity (see Figure 7d). This strain scale of order unity for stress to return to steady state is consistent with that found in the stop-and-go shearing discussed in section 3.1.

Figure 8a−d shows how the shear component of the fabric tensor, R_{xz}, evolved with strain for those systems in Figures 6a−d, respectively. Every time shear was reversed, the mean orientation of particles gradually changed. Like the shear stress, R_{xz} alternated between positive and negative values every time shear reversed directions as the particle contacts reversed their orientations. Analogous to both the normal and shear stresses, R_{xz} achieved the steady-state (plateau) value ($\approx \pm 0.14$) when $\varepsilon_{max} = 2$ (Figure 8d). Likewise, when ε_{max} was smaller (Figures 8a−c), R_{xz} did not reach a plateau value before shear was reversed. Furthermore, as observed in stop-and-go shearing, R_{xz} reached a plateau earlier ($\varepsilon' \approx 0.7$) than the stress did ($\varepsilon' \approx 1$). Again, this suggests that after the particles reach their steady mean orientation, shear must proceed farther for the force chains to be sufficiently built and rotated for the stress to reach its steady value.

In Figures 6−8, the results for all four values of κ collapsed onto the same curve. As such, the stress and microstructure evolutions with strain were rate-independent. This in turn means that the stress evolution did not depend on how much time has passed since shearing started in one direction, but rather on how far shear has proceeded in one direction. This is what was observed after shear was reversed during stop-and-go shearing.

Regardless if steady state was achieved, reversing shear then resulted in the normal stress dropping to a negative value, indicating that the system was in tension. This is not unlike what was observed when systems with strong force chains experienced a reversal of shear during stop-and-go shear. The normal stress grew again after the short-lived tensile state, and this whole pattern repeated ad infinitum. Similar transient negative normal stress was also observed in the suspension experiment by Kolli et al.,[18] and the mechanism is analogous to what is described here.

Figure 9a and b shows the effect of cohesion on the scaled normal stress and R_{xz} evolution, respectively. Results are shown for the oscillatory shear of systems with ε_{max} = 2 for three different levels of cohesion. The stresses in Figure 9a were cohesively scaled so that the steady state would be the same for all the systems, and by scaling this way, the stress evolution became independent of cohesion. The shear component of the fabric tensor, R_{xz}, shown in Figure 9b also showed no dependence on cohesion. These results again were also seen in stop-and-go shearing.

It was observed earlier in Figures 6−8 that when ε_{max} = 2, the stresses and the shear component of the fabric reached

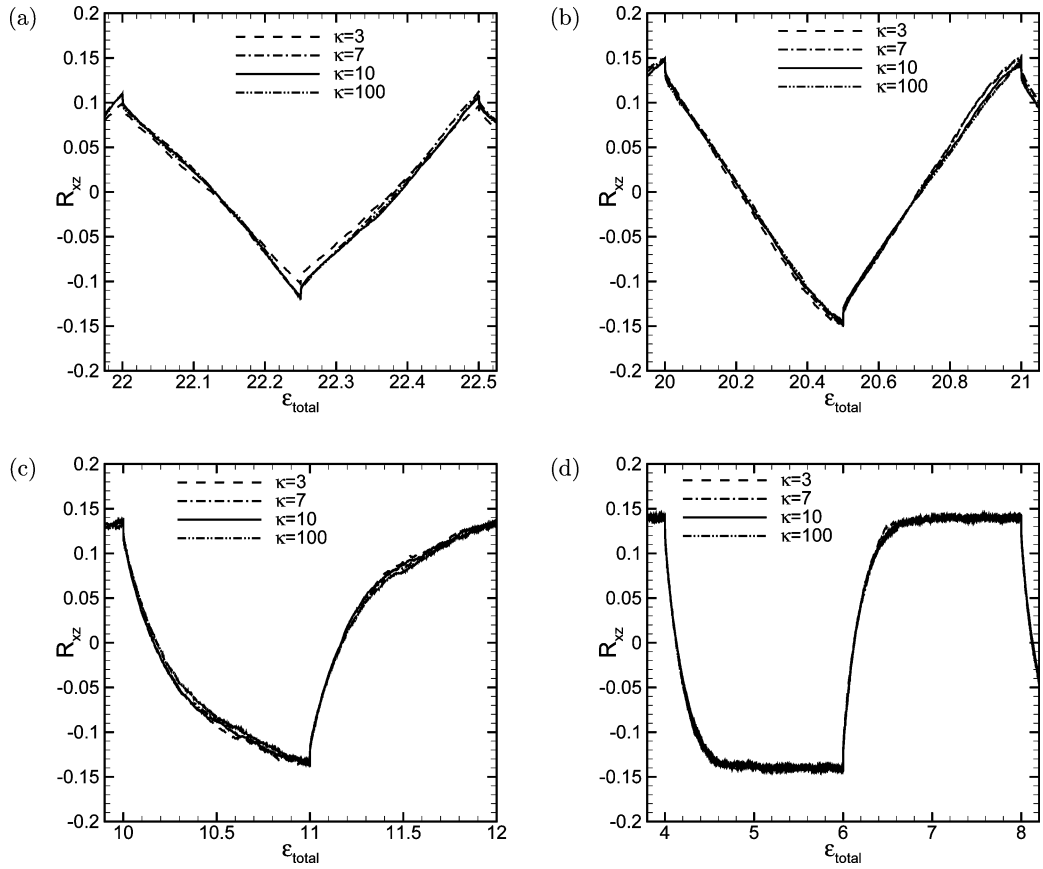

Figure 8. Strain dependence of the anisotropy for oscillatory shear with maximum strains of (a) ε_{max}= 0.25, (b) ε_{max}= 0.5, (c) ε_{max}= 1, and (d) ε_{max}= 2. Plotted is the shear component of the fabric tensor (R_{xz}) versus the total strain (ε_{total}). Each figure features the anisotropy evolution for four different values of the reduced minimum scaled stiffness (κ = 3, 7, 10, and 100). In all cases, ϕ = 0.6 and Bo^* = 2.5 × 10^{-5}.

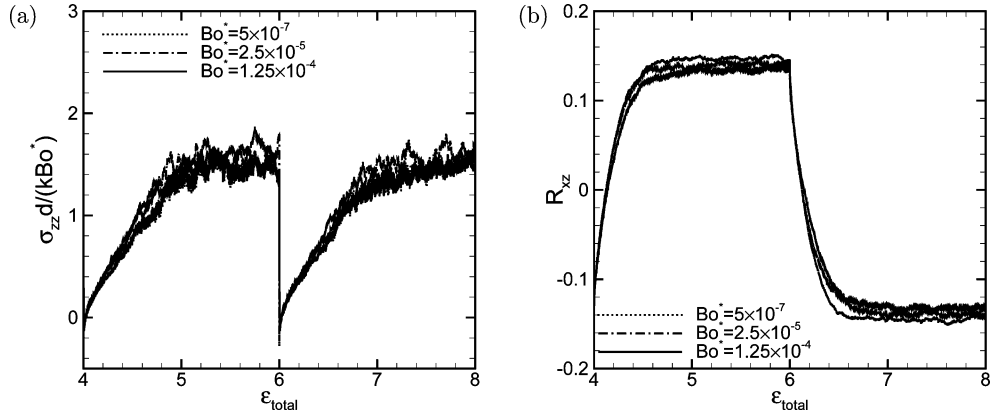

Figure 9. Effect of cohesion (Bo^*) on the behavior of the systems during oscillatory shear. Plotted are (a) the cohesively scaled normal stress ($\sigma_{zz}d/(kBo^*)$) and (b) the shear component of the fabric tensor (R_{xz}) versus the total strain (ε_{total}) for systems with three different levels of cohesion. In all cases, κ = 10, ε_{max}= 2, and ϕ = 0.6.

plateau values at a strain of about unity, but when ε_{max} = 1, such plateaus were not observed despite reaching a strain of unity. As such, the evolution of a system undergoing oscillatory shear depended on the ε_{max}. To better illustrate this, Figure 10a shows the stress evolution of systems undergoing oscillatory shear with two different strain amplitudes but the same shear-rate amplitude (since κ = 10 for both curves). It can be seen that the stress evolved at different incremental stiffness (dσ/dε) for the two different values of ε_{max} shown. As the system "was not aware" of how far shear would proceed before reversing, this dependence on ε_{max} must have come from a dependence on the shear history. If such dependence exists, then systems that share the same history but have different strain amplitudes would behave the same way until shear reversal and systems with different histories and strain amplitudes would not. Figure 10a shows the results after many oscillation cycles, and so, each system had a very different history; correspondingly, the stress behaved differently (compare the two curves between 22 < ε_{total} < 22.25). Figure 10b, in turn, shows the initial normal stress evolution for the same systems (in the very first oscillation cycle), starting from *the same system state*. The stress evolved identically for each strain amplitude until shear reversed direction; subsequently, each system evolved at a different incremental stiffness and, after many oscillation cycles, yielded Figure 10a. This contrast indicates that the stress response depends on the previous history but not on the shear rate. The

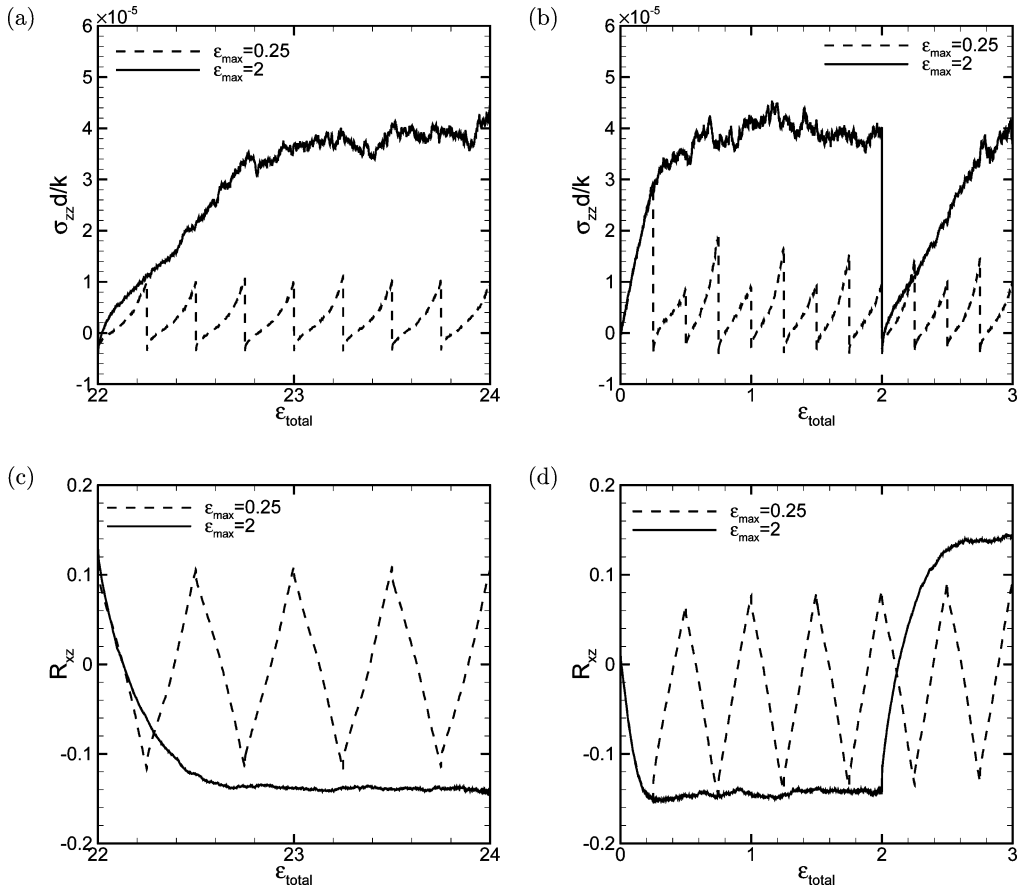

Figure 10. Effect of the strain amplitude on the evolution during oscillatory shear after shear has progressed for a long time (a and c) and during the initial oscillations (b and d). Plotted are the scaled normal stress ($\sigma_{zz}d/k$) and shear component of the fabric tensor (R_{xz}) versus the total strain (ε_{total}) for two different values of maximum strain (ε_{max}= 0.25 and 2). In all cases, $\phi = 0.6$, $Bo^* = 2.5 \times 10^{-5}$, and $\kappa = 10$.

history effect stems from the microstructure evolution as explained next. Furthermore, whereas for a given ε_{max} each half-oscillation was virtually identical to its previous one in Figure 10a, the same cannot be said during the initial oscillations shown in Figure 10b. Instead, when $\varepsilon_{max} < 1$, the stress alternated between evolving to a larger and smaller value every half-oscillation. Similar stress variation was also observed in the experiments of Toiya et al.[15] for small shear amplitudes. After many oscillation cycles, this behavior died out. This difference at the initial stage is also evidence of the history effect.

The history dependence just described above can be explained through examination of the evolution of the microstructure. Figure 10c and d show the behavior of R_{xz} for the same systems in Figure 10a and b, respectively. As mentioned before, when $\varepsilon_{max} = 2$, R_{xz} reached its plateau well before shear reversed, such that the internal structure was "fully in place" and the stress was able to build up to steady state. On the other hand, when $\varepsilon_{max} = 0.25$, R_{xz} did not get fully developed before reversal. This microstructure difference leads to the different stress response after reversal as observed. When shear was started in the first place, it was done so from a nearly isotropic configuration, i.e. R_{xz} was close to zero (see Figure 10d). In contrast, as seen in Figures 10c and 8, when shear was reversed after many cycles in oscillatory shear, R_{xz} was large, reflecting contact orientations corresponding to shear in the previous direction. This anisotropy difference leads to the different initial stress response (Figure 10b) from the steady state one (Figure 10a).

The behaviors observed for systems under oscillatory shear $\varepsilon_{max} = 2$ arose because steady state (in terms of stress and R_{xz}) was reached every time before shear was reversed. If that is all that mattered, then it would follow that the same behavior would be observed when the direction of shear is abruptly reversed in a simulation where the magnitude of shear is maintained constant. Note that in the oscillatory shear discussed above the shear rate changed sinusoidally; in contrast, we now hold the shear rate constant for a sufficiently long time to establish steady stress and fabric levels and then abruptly reverse the shear direction (as was done in Figure 5) after steady shear at steady state. Comparisons of the normal stress evolution after shear reversal for systems undergoing oscillatory shear with $\varepsilon_{max} = 2$ with systems reversed after a steady shear are shown in Figure 11a. (The figure display results for one-half of the oscillation cycle after several oscillation cycles to ensure that they represent long time solutions.) If the fluctuations were smoothed out, the normal stress behaved virtually identically for both types of shearing. The evolution of R_{xz} for these same systems is shown in Figure 11b. It can be seen that the microstructure also behaved virtually identically for both types of shearing. So as long as steady state (plateau) is achieved before shear is reversed, it does not matter how shear is performed; a sinusoidally varying shear rate would yield the same result as a square wave oscillation, etc. This further confirms that microstructure is the only cause of the history dependence in the quasi-static (rate-independent) regime.

The evolutions of normal and shear stresses following shear reversal observed in our simulations are consistent with the data from oscillatory shear experiments of Toiya et al.[15] In their study, beds of granular material were subjected to cylindrical Couette flow in which the direction of shear was repeatedly reversed. They observed that immediately after shear reversal,

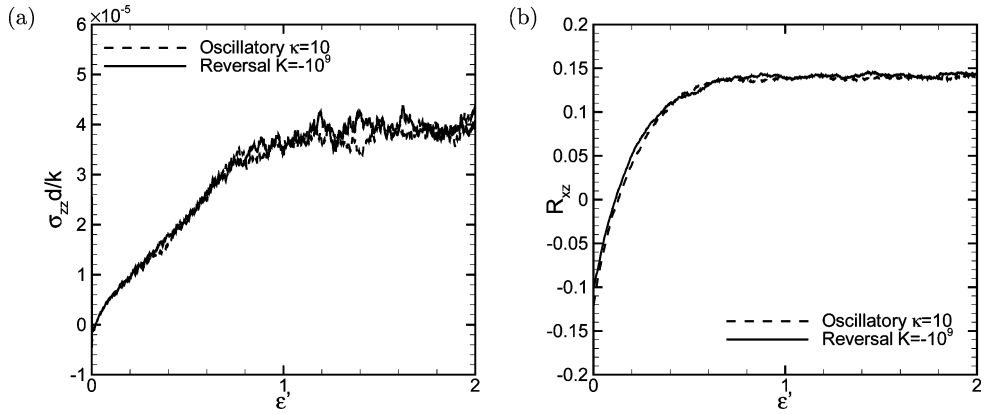

Figure 11. Comparison of evolutions resulting from reversing shear after steady state during different types of unsteady shear. Plotted are (a) the scaled normal stress ($\sigma_{zz}d/k$) and (b) the shear component of the fabric tensor (R_{xz}) versus the strain after shear is reversed (ε') for systems undergoing oscillatory shear with a strain amplitude $\varepsilon_{max} = 2$ (designated using the κ notation) and after steady shear (designated using the K notation). All simulations were performed with $\phi = 0.6$ and $Bo^* = 2.5 \times 10^{-5}$.

(a) the assembly compacted, which could happen only if the normal stress in a constant volume simulation decreased after shear reversal, (b) the magnitude of the shear stress first decreased and then recovered back to the old level, and (c) the torque achieved a steady value before the shear direction was reversed only when the maximum strain was sufficiently large.

3.4. Implications to Continuum Rheological Models. Virtually all continuum models for the rheology of dense assemblies in the quasi-static regime recognize and obey order-zero dependence on rate of deformation (D). Plasticity models have been proposed and adapted for granular materials.[22,23,44,45] These models satisfy such rate independence by expressing the stress as a function of $D/(D:D)^{1/2}$. The salient features of such plasticity models, when applied to simple shear of dense assemblies at constant volume conditions, are as follows:

(a) When an assembly under plane shear is subjected to any change in shear rate without reversing the direction of shear, the normal and shear stresses will not change; these are consistent with the *asymptotic* states observed in our simulations. These models miss the excursions observed in our simulations at very small strain levels; however, one may argue that these excursions are only of secondary importance and that the predictions of such order-zero, quasi-steady models as a simple first approximation.

(b) When an assembly under plane shear is subjected to shear reversal, the normal stresses will not change, while the shear stress will change sign *instantaneously*; these are again consistent with the *asymptotic* states observed in our simulations. However, our simulations indicate that all the stress components manifest significant dynamic changes following strain reversal that requires strain of order unity to stabilize.

Our simulations indicate that the fabric tensor is a natural metric of the microstructure anisotropy and that the stresses and the fabric evolve in a correlated manner. Thus, it seems reasonable to construct an evolution equation for the fabric and introduce an additional slow strain scale through it; the constitutive model for the stress is then revised to introduce the fabric tensor as additional variable. Goddard[30,31] has presented such an approach to model the stress evolution in dense suspensions and that Zhu et al.[46] have incorporated the effects of fabric in the dilatant double shearing model for granular materials.

4. Summary and Conclusions

In the present study, the responses of dense assemblies of cohesive granular materials to unsteady shear in the quasi-static regime have been investigated through DEM simulations. These simulations were performed in 3D periodic domains using Lees−Edwards boundary conditions and the SLLOD algorithm. The dynamic characteristics of the volume-averaged normal and shear stresses in materials sheared at constant volume, undergoing stop-and-go shearing and oscillatory shear, are discussed in detail. Furthermore, the evolution of microstructure anisotropy has been quantified through the shear component of the fabric tensor and related to the dynamic characteristics of the stress components.

It has been demonstrated that the evolution of the stresses and the microstructure anisotropy depended on the strain extent, but not on the shear rate. Therefore, the results in this paper confirm that cohesive granular materials can exhibit quasi-static rheological behaviors even if subjected to unsteady shear. The cohesive scaling, which collapses systems of different cohesion levels into a universal quasi-static regime under steady shear[13] has been extended to and validated for the unsteady shear.

The stresses and the microstructure anisotropy undergo a transition following reversal of shear direction, which requires a shear strain of about unity to fully adapt. In contrast, they reach the previous steady state values rapidly when shear is resumed in the same direction. This characteristic strain of about unity is a robust length scale independent of shear-rate, volume fraction, and cohesion strength. These results clearly establish a correlation between the stress evolution and the microstructure anisotropy development. When shear was completely stopped, the stress experienced an almost immediate decrease, depending mostly on the stability of the microstructure beforehand, which could roughly be quantified using the average coordination number.

It is pointed out that continuum rheological models for dense assemblies of particles deforming in the quasi-static regime capture the asymptotic behavior of the stresses following dynamic changes in the rate of deformation, but not the dynamic events occurring immediately following changes. An augmented plasticity model, which introduces an additional slow strain scale via a dynamic model for the evolution of the fabric tensor, is suggested as a natural extension of the extant plasticity model to bring the model predictions closer to our simulation results.

Acknowledgment

This work was partially supported by Merck & Co., Inc., an NSF-NIRT grant, and a DOE-UCR grant with award number DE-FG26-07NT43070.

Literature Cited

(1) Lätzel, M.; Luding, S.; Herrmann, H. J. Macroscopic material properties from quasi-static, microscopic simulations of a two-dimensional shear-cell. *Granular Matter* **2000**, *2* (3), 123–135.

(2) da Cruz, F.; Emam, S.; Prochnow, M.; Roux, J.-N.; Chevoir, F. Rheophysics of dense granular materials: Discrete simulation of plane shear flows. *Phys. Rev. E* **2005**, *72* (2), 021309–17.

(3) Lois, G.; Lemaître, A.; Carlson, J. M. Numerical tests of constitutive laws for dense granular flows. *Phys. Rev. E* **2005**, *72* (05), 051303−051303.

(4) Silbert, L. E.; Grest, G. S.; Brewster, R.; Levine, A. J. Rheology and Contact Lifetimes in Dense Granular Flows. *Phys. Rev. Lett.* **2007**, *99* (6), 068002–4.

(5) Rognon, P. G.; Roux, J.-N.; Naaïm, M.; Chevoir, F. Dense flows of cohesive granular materials. *J. Fluid Mech.* **2008**, *596* (−1), 21–47.

(6) Miller, B.; O'Hern, C.; Behringer, R. P. Stress fluctuations for continuously sheared granular materials. *Phys. Rev. Lett.* **1996**, *77* (15), 3110–3113.

(7) Bocquet, L.; Losert, W.; Schalk, D.; Lubensky, T. C.; Gollub, J. P. Granular shear flow dynamics and forces: Experiment and continuum theory. *Phys. Rev. E* **2001**, *65* (1), 011307.

(8) Tardos, G. I.; McNamara, S.; Talu, I. Slow and intermediate flow of a frictional bulk powder in the Couette geometry. *Powder Technol.* **2003**, *131* (1), 23–39.

(9) MiDi, G. D. R. On dense granular flows. *Eur. Phys. J. E, Soft Matter* **2004**, *14* (4), 341–305.

(10) Majmudar, T. S.; Behringer, R. P. Contact force measurements and stress-induced anisotropy in granular materials. *Nature* **2005**, *435* (1079), 1079–1082.

(11) Campbell, C. S. Granular shear flows at the elastic limit. *J. Fluid Mech.* **2002**, *465*, 261–291.

(12) Campbell, C. S. Stress-controlled elastic granular shear flows. *J. Fluid Mech.* **2005**, *539*, 273–297.

(13) Aarons, L.; Sundaresan, S. Shear flow of assemblies of cohesive and non-cohesive granular materials. *Powder Technol.* **2006**, *169* (1), 10–21.

(14) Aarons, L.; Sundaresan, S. Shear flow of assemblies of cohesive granular materials under constant applied normal stress. *Powder Technol.* **2008**, *183* (3), 340–355.

(15) Toiya, M.; Stambaugh, J.; Losert, W. Transient and Oscillatory Granular Shear Flow. *Phys. Rev. Lett.* **2004**, *93* (8), 088001–4.

(16) Mueggenburg, N. W. Behavior of granular materials under cyclic shear. *Phys. Rev. E* **2005**, *71* (3), 031301–10.

(17) Gadala-Maria, F.; Acrivos, A. Shear-induced structure in a concentrated suspension of solid spheres. *J. Rheol.* **1980**, *24* (6), 799–814.

(18) Kolli, V. G.; Pollauf, E. J.; Gadala-Maria, F. Transient normal stress response in a concentrated suspension of spherical particles. *J. Rheol.* **2002**, *46* (1), 321–334.

(19) Narumi, T.; See, H.; Honma, Y.; Hasegawa, T.; Takahashi, T.; Phan-Thien, N. Transient response of concentrated suspensions after shear reversal. *J. Rheol.* **2002**, *46* (1), 295–305.

(20) Narumi, T.; See, H.; Suzuki, A.; Hasegawa, T. Response of concentrated suspensions under large amplitude oscillatory shear flow. *J. Rheol.* **2005**, *49* (1), 71–85.

(21) Utter, B.; Behringer, R. P. Transients in sheared granular matter. *Eur. Phys. J. E, Soft Matter* **2004**, *14* (4), 373–380.

(22) Savage, S. B. Granular flow down rough inclines-review and extension. In *Mechanics of granular materials: new models and constitutive relations*; Jenkins, J. T., Satake, M., Eds.; Elsevier Ltd: New York, 1983.

(23) Schaeffer, D. G. Instability in the evolution equations describing incompressible granular flow. *J. Differential Equat.* **1987**, *66*, 19–50.

(24) Schofield, A. a.; Peter, W. *Critical State Soil Mechanics*; McGraw-Hill Inc.: New York, 1968.

(25) Kolymbas, D. *Introduction to Hypoplasticity*; A. A. Balkema, Rorrerdam, 2000.

(26) Bathurst, R. J.; Rothenburg, L. Observations on stress-force-fabric relationships in idealized granular materials. *Mech. Mater.* **1990**, *9* (1), 65–80.

(27) Radjai, F.; Wolf, D. E.; Jean, M.; Moreau, J.-J. Bimodal Character of Stress Transmission in Granular Packings. *Phys. Rev. Lett.* **1998**, *80*, (1), 61−74.

(28) Deboeuf, S.; Dauchot, O.; Staron, L.; Mangeney, A.; Vilotte, J.-P. Memory of the unjamming transition during cyclic tiltings of a granular pile. *Phys. Rev. E* **2005**, *72* (5), 051305–11.

(29) Nemat-Nasser, S. A micromechanically-based constitutive model for frictional deformation of granular materials. *J. Mech. Phys. Solids* **2000**, *48* (6−7), 1541–1563.

(30) Goddard, J. D. A dissipative anisotropic fluid model for non-colloidal particle dispersions. *J. Fluid Mech.* **2006**, *568* (−1), 1–17.

(31) Goddard, J. D. A weakly nonlocal anisotropic fluid model for inhomogeneous Stokesian suspensions. *Phys. Fluids* **2008**, *20* (4), 040601–16.

(32) Cundall, P. A.; Strack, O. D. L. A discrete numerical model for granular assemblies. *Geotechníque* **1979**, *29* (1), 47–65.

(33) Campbell, C. S. Granular Shear Flows at the Elastic Limit. *J. Fluid Mech.* **2002**, *465*, 261–291.

(34) Stevens, A. B.; Hrenya, C. M. Comparison of soft-sphere models to measurements of collision properties during normal impacts. *Powder Technol.* **2005**, *154*, 99–109.

(35) Vu-Quoc, L.; Zhang, X. An Accurate and Efficient Tangential Force-Displacement Model for Elastic Frictional Contact in Particle-Flow Simulations. *Mech. Mater.* **1999**, *31* (4), 235–269.

(36) Walton, O. R.; Braun, R. L. Viscosity, Granular-Temperature, and Stress Calculations for Shearing Assemblies of Inelastic, Frictional Disks. *J. Rheol.* **1986**, *30* (5), 949–980.

(37) Yang, R. Y.; Zou, R. P.; Yu, A. B. Computer simulation of the packing of fine particles. *Phys. Rev. E* **2000**, *62* (3), 3900–3908.

(38) Seville, J. P. K.; Willett, C. D.; Knight, P. C. Interparticle forces in fluidisation: a review. *Powder Technol.* **2000**, *113* (3), 261–268.

(39) Lees, A. W.; Edwards, S. F. The computer study of transport processes under extreme conditions. *J. Phys. C: Solid State Phys.* **1972**, *5* (15), 1921–1928.

(40) Evans, D. J.; Morriss, G. P. *Statistical Mechanics of Nonequilibrium Liquids*; Academic Press: New York, 1990.

(41) Plimpton, S. J. Fast parallel algorithms for short-range molecular dynamics. *J. Comp. Phys.* **1995**, *117*, 1–19.

(42) Bricker, J. M.; Butler, J. E. Correlation between stresses and microstructure in concentrated suspensions of non-Brownian spheres subject to unsteady shear flows. *J. Rheol.* **2007**, *51* (4), 735–759.

(43) Ball, R. C.; Blumenfeld, R. Stress field in granular systems: Loop forces and potential formulation. *Phys. Rev. Lett.* **2002**, *88*, 115505.

(44) Goddard, J. D. Dissipative materials as models of thixotropy and plasticity. *J. Non-Newtonian Fluid Mech.* **1984**, *14*, 141–160.

(45) Srivastava, A.; Sundaresan, S. Analysis of a frictional-kinetic model for gas-particle flow. *Powder Technol.* **2003**, *129*, 72–85.

(46) Zhu, H.; Mehrabadi, M. M.; Massoudi, M. Three-dimensional constitutive relations for granular materials based on the dilatant double shearing mechanism and the concept of fabric. *Int. J. Plasticity* **2006**, *22* (5), 826–857.

Received for review July 26, 2009
Revised manuscript received October 17, 2009
Accepted October 20, 2009

IE901187W